

M-DWARF FAST ROTATORS AND THE DETECTION OF RELATIVELY YOUNG MULTIPLE M-STAR SYSTEMS

S. RAPPAPORT¹, J. SWIFT², A. LEVINE³, M. JOSS¹, R. SANCHIS-OJEDA¹, T. BARCLAY⁴,
M. STILL⁴, G. HANDLER⁵, K. OLÁH⁶, P. S. MUIRHEAD^{7,8}, D. HUBER⁹, AND K. VIDA⁶

Draft version May 8, 2014

ABSTRACT

We have searched the *Kepler* light curves of ~ 3900 M-star targets for evidence of periodicities that indicate, by means of the effects of starspots, rapid stellar rotation. Several analysis techniques, including Fourier transforms, inspection of folded light curves, ‘sonograms’, and phase tracking of individual modulation cycles, were applied in order to distinguish the periodicities due to rapid rotation from those due to stellar pulsations, eclipsing binaries, or transiting planets. We find 178 *Kepler* M-star targets with rotation periods, P_{rot} , of < 2 days, and 110 with $P_{\text{rot}} < 1$ day. Some 30 of the 178 systems exhibit two or more independent short periods within the same *Kepler* photometric aperture, while several have three or more short periods. Adaptive optics imaging and modeling of the *Kepler* pixel response function for a subset of our sample support the conclusion that the targets with multiple periods are highly likely to be relatively young physical binary, triple, and even quadruple M star systems. We explore in detail the one object with four incommensurate periods all less than 1.2 days, and show that two of the periods arise from one of a close pair of stars, while the other two arise from the second star, which itself is probably a visual binary. If most of these M-star systems with multiple periods turn out to be bound M stars, this could prove a valuable way of discovering young hierarchical M-star systems; the same approach may also be applicable to G and K stars. The $\sim 5\%$ occurrence rate of rapid rotation among the ~ 3900 M star targets is consistent with spin evolution models that include an initial contraction phase followed by magnetic braking, wherein a typical M star can spend several hundred Myr before spinning down to periods longer than 2 days.

Subject headings: techniques: photometric—stars:activity—binaries (including multiple)—binaries: general—stars: late type—stars: rotation—stars: spots

1. INTRODUCTION

M dwarfs—main-sequence stars with masses $M_{\star} \lesssim 0.6 M_{\odot}$ —dominate the Galactic stellar population in number and mass (Chabrier 2003). This preponderance is reflected in the local neighborhood where $\sim 75\%$ of the nearest stars fall within this spectral class (Henry et al. 1994, 2006; Reid et al. 2002; Cruz & Reid 2002), and this fraction will continue to grow as more nearby red dwarfs are revealed. Despite their ubiquity, these small stars are difficult to characterize due in part to their low luminosities and complex atmospheres, and models are

unable to satisfactorily account for their radii and temperatures at given masses (Torres et al. 2010; Boyajian et al. 2012; Birkby et al. 2013). The motivation to understand the fundamental properties of M dwarfs, including their multiplicity, has been amplified by recent results indicating that they frequently host low-mass planets (Swift et al. 2013; Dressing & Charbonneau 2013; Morton & Swift 2013).

Low-mass stars lose angular momentum through rotational magnetic braking (Mestel 1968). However, during their pre-main sequence lifetime their rotation rates increase due to gravitational contraction. This pre-main sequence phase can last from ~ 100 Myr for stars of mass $0.5 M_{\odot}$ to several hundred Myr for the lowest mass stars (see, e.g., Baraffe et al. 2002). After hydrogen burning commences in their cores and gravitational contraction ceases these stars begin to gradually spin down. Consequently, their magnetic field strengths and activity levels tend to decline (Skumanich 1972).

M dwarfs are thought to rotate differentially, but less so than solar type stars. Recent measurements based on *Kepler* data show that differential rotation rates for M dwarfs are typically less than 0.1 rad d^{-1} (Reinhold et al. 2013). Observations of late type stars show that their differential rotation rates generally depend strongly on effective temperature and weakly on rotation period (Barnes et al. 2005; Reiners 2006), a behavior that is also seen in computer models (Küker & Rüdiger 2011).

The *Kepler* Space Mission (Borucki et al. 2010; Koch et al. 2010) monitored over 150,000 stars nearly continuously for about four years, primarily to search for exo-

¹ Department of Physics, and Kavli Institute for Astrophysics and Space Research, Massachusetts Institute of Technology, Cambridge, MA 02139, USA; sar@mit.edu, mattjoss@mit.edu, rsanchis86@gmail.com

² Department of Astronomy and Department of Planetary Science, California Institute of Technology, MC 249-17, Pasadena, CA 91125, USA; jswift@astro.caltech.edu

³ 37-575 M.I.T. Kavli Institute for Astrophysics and Space Research, 70 Vassar St., Cambridge, MA, 02139; aml@space.mit.edu

⁴ BAER Institute/NASA Ames Research Center, M/S 244-30, Moffett Field, Mountain View, California 94035; thomas.barclay@nasa.gov, martin.d.still@nasa.gov

⁵ Nicolaus Copernicus Astronomical Center, Bartycka 18, PL 00-716 Warsaw, Poland; gerald@camk.edu.pl

⁶ Konkoly Observatory of the Hungarian Academy of Sciences, PO Box 67, H-1525 Budapest, Hungary; olah@konkoly.hu; vidakris@konkoly.hu

⁷ Department of Astronomy, Boston University, Boston, MA 02215; philipm@bu.edu

⁸ Hubble Postdoctoral Fellow

⁹ SETI Institute/NASA Ames Research Center, MS 244-30, Moffett Field, CA 94035, USA; daniel.huber@nasa.gov

planets (Borucki et al. 2011; Batalha et al. 2013; Burke et al. 2013). *Kepler*'s unprecedented photometric precision has also led to extensive ancillary investigations¹⁰.

Though the vast majority of *Kepler* target stars are Sun-like ($0.8 \lesssim M_{\star} \lesssim 1.2 M_{\odot}$), several thousand M dwarfs have been monitored as well over the course of the primary mission. The initial estimation of the important characteristics of the stars in the *Kepler* field was done using ground-based multicolor photometry as part of the construction of the *Kepler* Input Catalog (KIC). This estimation process was optimized for sun-like stars; the characteristics of the M dwarfs in the KIC were not determined as accurately and should be adopted only with caution (Brown et al. 2011). There have been several efforts to revise the stellar parameters for this M-star sample (e.g. Muirhead et al. 2012a; Mann et al. 2012, 2013). In particular, Dressing & Charbonneau (2013; hereafter ‘‘DC13’’) have tabulated and calibrated the properties of 3897 cool and high surface gravity *Kepler* target stars. The vast majority of these have masses in the range $0.3 < M_{\star} < 0.6 M_{\odot}$ and the bulk of the effective temperatures fall in the range $3300 < T_{\text{eff}} < 4000$ K. The numbers of stars show a bias toward the higher mass M dwarfs due to the magnitude limited nature of the *Kepler* targets (Batalha et al. 2010). Some 90% of the DC13 collection of M stars are at distances in the range 15-400 pc (median distance of 210 pc), and have absolute visual magnitudes in the range +8 to +12.

McQuillan, Aigrain, & Mazeh (2013) performed both autocorrelation function (‘‘ACF’’) and Fourier transform analyses of the *Kepler* photometric data for the M dwarf targets in order to identify variations of the stellar fluxes due to starspots and to measure the corresponding periods. The period distribution that they derived is shown in the top panel of Fig. 1. The distribution includes periods all the way down to less than a day, has local maxima near 19 days and 33 days, and tails off dramatically toward periods above 40 days. There is also what appears to be a distinct group of M stars with periods less than ~ 6 days, and the distribution is rising toward the shortest periods. Some 55 of these M stars have rotation periods of $\lesssim 2$ days.

In this work we focus on the rapidly rotating M stars, in particular those with $P_{\text{rot}} < 1$ day. In Section 2 we describe our search through the *Kepler* photometric data base for rapidly rotating M stars using a Fourier transform algorithm. In Section 3 the possibility that some of the periodicities we observe are due to stellar pulsations is discussed and largely discounted. We show selected examples of ‘‘sonograms’’ for several of our candidate rotators in Section 4, and demonstrate that various frequencies and their harmonics appear to vary independently, thereby arguing for the rotating spotted star hypothesis. In Section 5 we present an analysis where we track the phases of individual starspot rotation cycles and thereby demonstrate that these are not stellar pulsations. In Section 6 we discuss the *Kepler* M-star targets wherein we have found two or more distinct rotation periods. This includes some 30 with at least two short periods, several with three periods, and one with four distinct periods (all shorter than 1.2 days). We argue in Section 7 that these

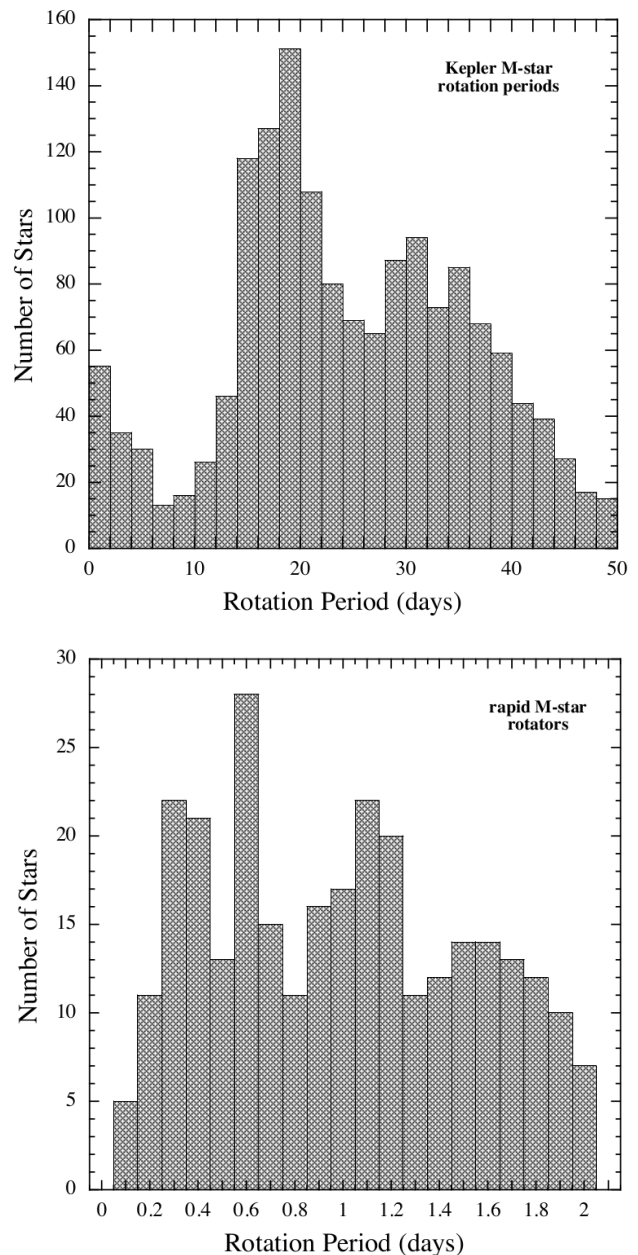


FIG. 1.— Top: Rotation period distribution of M stars in the *Kepler* data set; the periods were taken from McQuillan et al. (2013), and are based on 10 months of data. Note the distinct group of relatively rapid rotators with periods shorter than ~ 5 days. Bottom: Distribution of very short rotation periods found in *Kepler* M-star targets via our Fourier transform search of all 16 quarters of data. In the case of multiple periods in a single *Kepler* target, we include *all* the periods in this histogram.

are actually binary, triple, and quadruply bound M-star systems. In Section 8, we present evidence, based on UKIRT J-band and Keck adaptive optics images, that these are indeed binary and/or hierarchical systems. In Section 9 we apply a point-spread-function analysis to the *Kepler* pixel-level data for KIC 4660255 which exhibits four short periodicities, and show that two of them arise in each of two stellar images separated by about $4''$. We summarize our results and draw some final conclusions in Section 10.

¹⁰ keplerscience.arc.nasa.gov/PublicationsAstrophysics.shtml

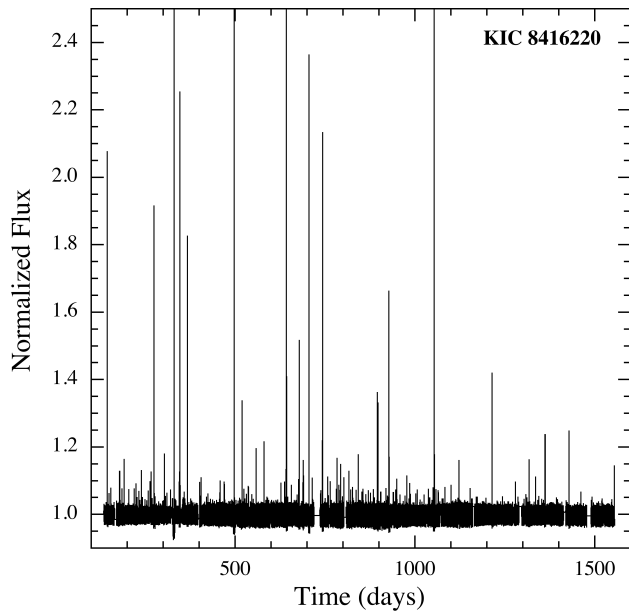
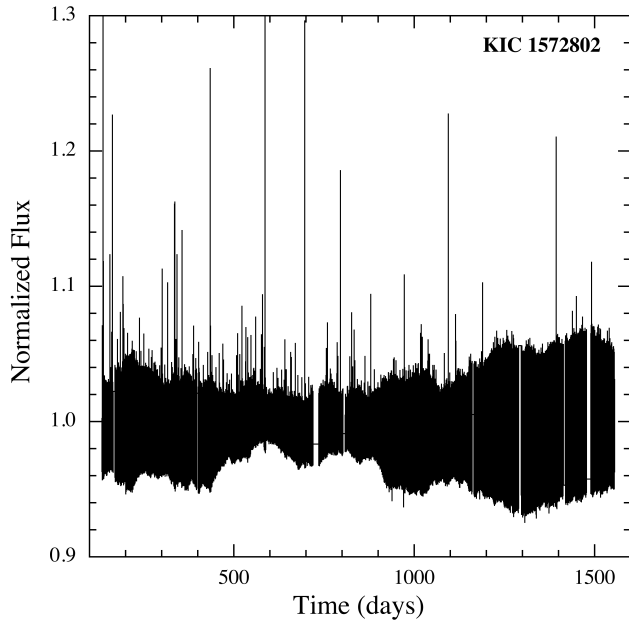


FIG. 2.— Illustrative *Kepler* light curves of M-stars. Top: KIC 1572802 which exhibits flares as large as $\sim 30\%$ of the mean stellar flux, and one periodicity of 0.37 days. Bottom: KIC 8416220, which has two periods of 0.72 and 0.57 days, and exhibits flares that increase the flux by a whole magnitude.

2. SEARCH FOR RAPIDLY ROTATING M STARS

Because the Fourier transform (‘FT’) is an efficient tool for searching for periodic signals with high-duty cycle and smoothly varying profiles (i.e., where the first few harmonics dominate), it was our choice for discovering spotted stars rotating with short periods. While the transitory nature of starspots, which can induce possible erratic changes in the modulation phase, and surface differential rotation can broaden the peaks in a Fourier power spectrum, we did not find it necessary, nor particularly useful, to employ an ACF analysis. As it turns out, we have discovered a substantial number of *Kepler* M-star targets that exhibit more than one indepen-

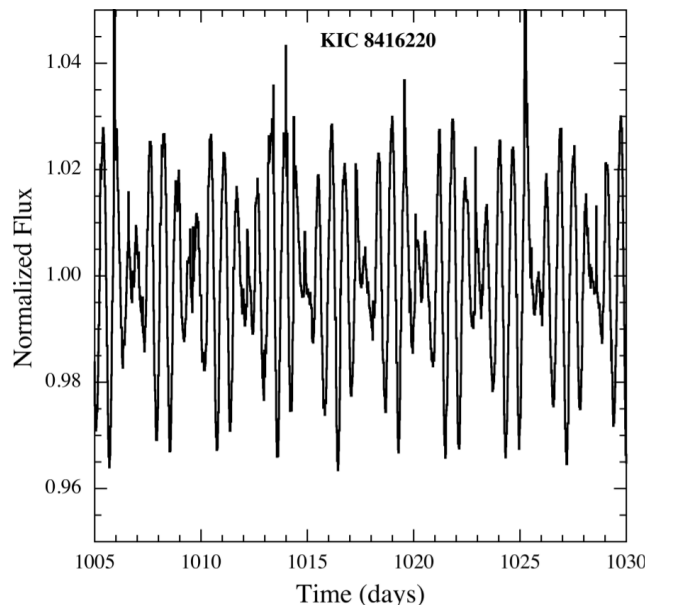
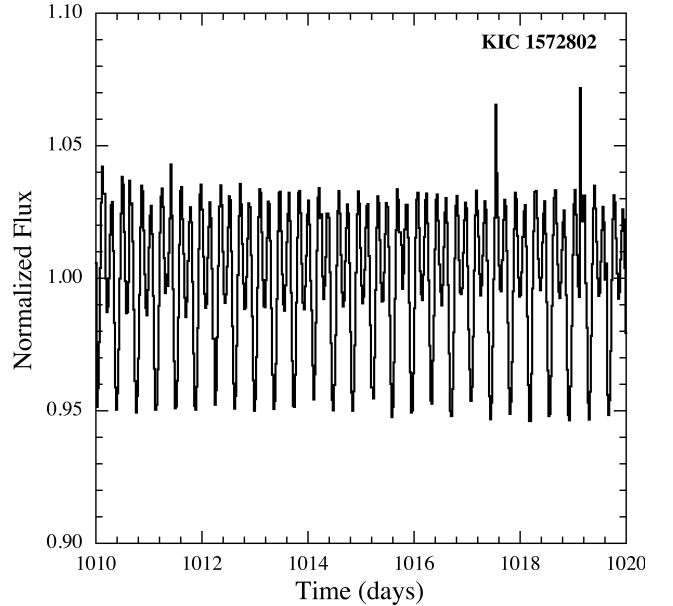


FIG. 3.— Short segments of the light curves for KIC 1572802 and KIC 8416220 shown in Fig. 2. Top: The structure in the light curve of KIC 1572802 results from a single periodicity, but with higher harmonic structure (see Fig. 4). Bottom: The structure in the light curve of KIC 8416220 results from the beat of two periodicities that differ by $\sim 23\%$ (see Fig. 4).

dent period—sometimes close to or near multiples of one another—and the FT is substantially more straightforward than an ACF to use in identifying multiple periods.

The FT approach utilized in this work is very similar in nature to the one used by Sanchis-Ojeda et al. (2013) in their search for short-period planets, and is based on the same selection criteria. In brief, the available *Kepler* PD-CSAP_FLUX data (corrected with PDCMAP; Stumpe et al. 2012; Smith et al. 2012) were normalized quarter-by-quarter with the quarterly median values and then stitched together into a single data file, with all data gaps filled with the mean flux. After the FTs were computed, *amplitude* spectra were produced with units of parts per million (ppm) variation with respect to a flux of unity.

We refer to these Fourier transforms below simply as “the FT”. For the purpose of searching for statistically significant peaks, we further normalized the FT by dividing by a smoothed version of the FT. The smoothing was accomplished by convolution with a boxcar function that is 100 frequency bins in length. This procedure has the effect of normalizing the raw FT to its local (100-bin) mean. All targets whose normalized FT revealed at least one frequency peak exceeding the local mean by a factor > 4 with at least one harmonic or subharmonic which exceeded its local mean by a factor of 3, were considered to be worthy of further investigation. We note that the analysis outlined here of the 3897 DC13 M-star *Kepler* targets requires only about one hour of cpu time on a standard laptop machine.

In all, we find 297 of the 3897 targets exhibit the requisite significant FT signal comprising a base frequency plus its harmonic, with the base frequency exceeding 0.5 cycles/day (i.e., $P_{\text{rot}} < 2$ days). We believe that the majority of these periodicities are likely to be due to stellar rotation manifested via starspots, but a significant number may be due to planet transits and binary eclipses. The individual FTs for these systems were further examined to eliminate those which were clearly not due to rotating starspots. In all cases we folded the data modulo the detected fundamental period, and were readily able to rule out cases due to transiting planets since their well-known sharp, relatively rectangular dipping profiles are characteristic. Of course, we also checked the KOI list for matches. Any of the objects that appear in the *Kepler* eclipsing binary (“EB”) star catalog (e.g., Matijević et al. 2012) were likewise eliminated.

Spots on a rotating star can, depending on their locations and other properties, produce a profile that may be mistaken for the profile of an EB. The target KIC 1572802 is an example; see the top panel of Fig. 3. It exhibits variations at a period of 8.9 hours that resemble the light curve of a contact binary. However, an inspection of the top panel in Fig. 2, which shows the corresponding full *Kepler* light curve, indicates that the object is not likely to be a contact binary. Aside from the profusion of stellar flares, which are not atypical of M stars, the overall envelope of the 8.9-hour periodicity is seen to be highly and erratically variable. These amplitude changes are inconsistent with the behavior of a typical EB. Moreover, the shape of the 8.9-hr modulation changes dramatically over the four years of observations. The Fourier transform for this object is shown in the top left panel of Fig. 4.

The bottom panels of Figs. 2 and 3 provide another example, i.e., the M star KIC 8416220 that exhibits a non-EB like light curve, yet where the overall amplitude remains nearly constant over the long term. This light curve results from a beat between two rotation periodicities whose periods differ by only $\sim 20\%$ (see the FT in the upper right panel of Fig. 4).

After carefully examining the 297 M star targets that exhibit significant periodicities with periods less than two days, we believe we have identified the stellar rotators, and are able to exclude the eclipsing binaries and transiting planets. In summary, we find that approximately 110 of these are previously identified binaries or transiting planets, or are likely to be binaries or transiting planets based on the characteristics of their FTs or folded

light curves. Some eight of the 297 targets were identified as artifacts caused by leakage of the signal from the very bright star RR Lyr that pulsates with a period of 0.5669 days. After elimination of these targets, there remain 178 targets that exhibit one or more periodicities that are likely to be due to starspots (see Table 1) on rotating stars. These targets comprise a total of 211 different periodicities with $P_{\text{rot}} \lesssim 2$ days. Some 110 of the 178 targets exhibit 127 periodicities with $P_{\text{rot}} \lesssim 1$ day. The distribution of all 211 periods is shown in the bottom panel of Fig. 1.

3. POSSIBLE STELLAR PULSATIONS AMONG THE PERIODICITIES

Stars with convective envelopes oscillate in multiple modes that are typically manifest as a forest of peaks in a Fourier spectrum, with amplitudes forming a roughly Gaussian-shaped envelope (see, e.g., Bedding 2011 for a recent review). The frequency of the mode with the maximum amplitude, ν_{max} , has been proposed to scale with the acoustic cut-off frequency (Brown et al. 1991) and can be related to basic stellar parameters by the scaling relation (Kjeldsen & Bedding 1995):

$$\frac{\nu_{\text{max}}}{\nu_{\text{max},\odot}} = \frac{M/M_{\odot}}{(R/R_{\odot})^2 \sqrt{(T_{\text{eff}}/5777\text{K})}} \quad (1)$$

Using the masses, effective temperatures, and radii of *Kepler* M-star targets as determined by Dressing & Charbonneau (2013), as well as $\nu_{\text{max},\odot} \simeq 3140 \mu\text{Hz}$ (Barban et al. 2013), this relation yields ν_{max} values in the range 6.4 - 31.6 mHz, corresponding to periods between 0.5 and 2.6 minutes. This is at least a factor of 80 shorter than the shortest period in our stellar sample. Additionally, scaling relations for amplitudes of convectively excited oscillations predict amplitudes lower than a few parts per million for M dwarfs (Corsaro et al. 2013), which is incompatible with our observations. This, in combination with the lack of the typical Gaussian-shaped forests of peaks in our Fourier transforms, argues strongly against solar-like oscillations as the cause of the observed variability.

On the other hand, pulsations driven by the ϵ mechanism and convective-flux blocking similar to those in γ Doradus variables have been theoretically predicted to occur in M dwarfs (Rodríguez-López et al. 2012, 2013). Usually, the associated pulsation periods would be of the order of half an hour, but for some low-mass pre-main sequence models timescales between 7 - 11 hours were found. However, the authors argued that these oscillations would only grow during the short phase of deuterium burning, and, furthermore, would only grow slowly during that phase. It thus seems unlikely that pulsations driven by this mechanism could be responsible for the observed periodicities. Further evidence against contamination of our sample by stellar pulsations is provided in Sections 4 and 5.

4. TIME-FREQUENCY (“SONOGRAM”) ANALYSIS

As a further check as to whether the periodicities in the *Kepler* M-star data are the result of the rotation of spotted stars, we have also carried out sonogram, i.e., time-frequency, analyses. In the present case, short segments of the *Kepler* time series are Fourier transformed

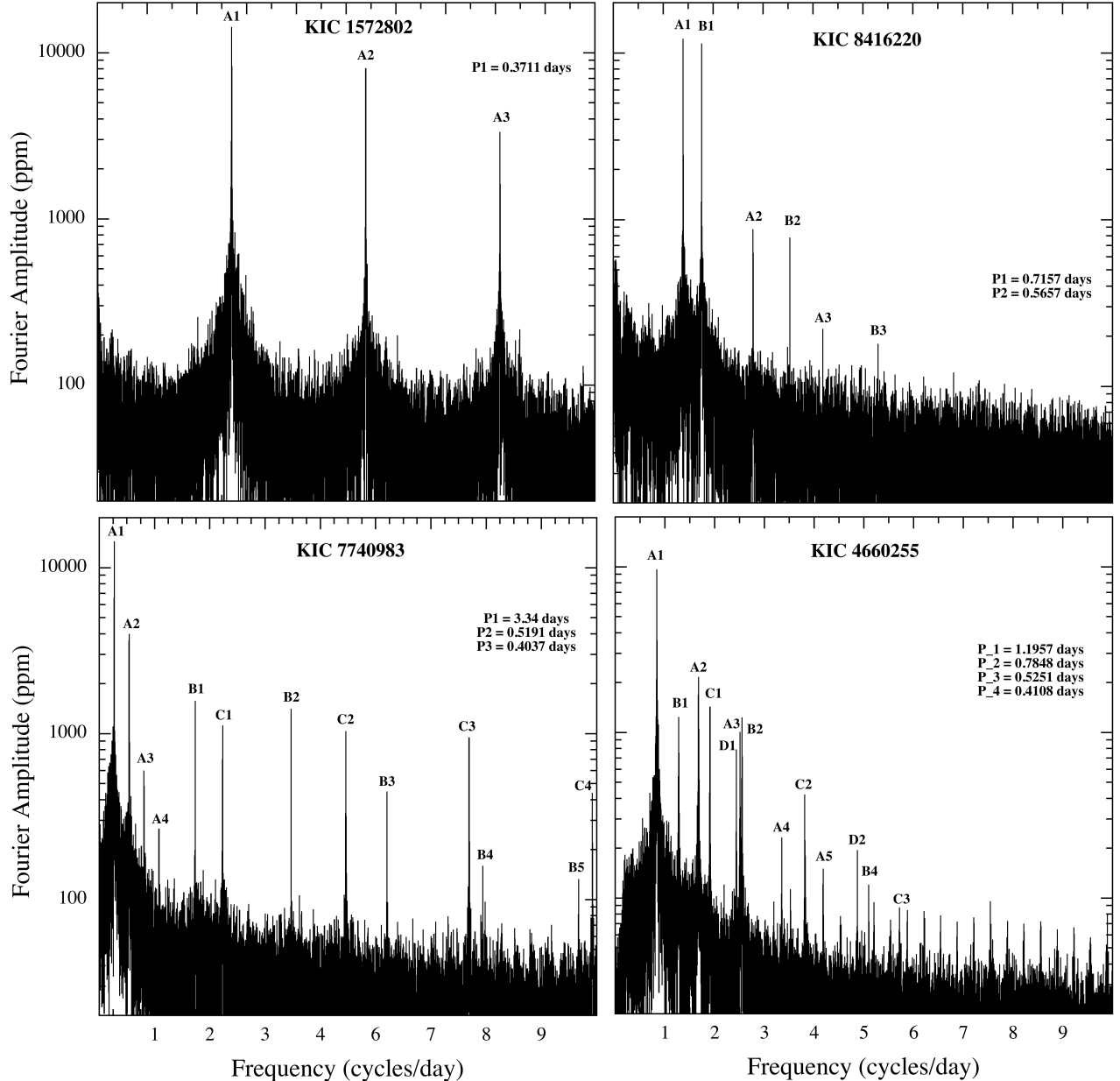


FIG. 4.— Four illustrative Fourier transforms of *Kepler* M-star targets. KIC 1572802 has a single short rotation period; KIC 8416220 has two periods; KIC 7740983 has three; and KIC 4660255 has four rotation periods of < 1 day. The letters near the peaks designate one of the different periods, while the number which follows indicates the harmonic number – starting with 1 for the base frequency. The sequence of peaks in KIC 4660255 above frequencies of 6 cycles day^{-1} and spaced by $1/3$ cycle day^{-1} is an artifact of the *Kepler* momentum wheel.

and the amplitudes in each FT are displayed as a function of frequency in a vertical linear strip of a two-dimensional image. The orthogonal coordinate of the image encodes the start times of the data segments. The duration of the individual segments of the time series, and their overlap are parameters that can be adjusted. The image shows how the amplitude of a particular signal evolves with time.

To compute the sonograms, we used the program package *TiFrAn* (Time Frequency Analysis; Kolláth & Oláh 2009) which allows a time-frequency analysis to be carried out via several different methods. From these possible options, we have chosen the Short-Term Fourier Transform (STFT) to study the rotational periodicities.

This procedure yields good resolution in both time and frequency. In particular, each data segment is defined by a Gaussian window function with full width at half maximum (FWHM) of about 30 days, and the centers of the windows of sequential segments are separated by ~ 2 days.

In Fig. 5 we show sonograms for the same four *Kepler* targets whose full FTs are displayed in Fig. 4. The FT amplitudes of most of the individual frequency components appear to change dramatically and erratically over time, and largely independently of one another. This gives added weight to the hypothesis that these are indeed features due to spots on rotating stars, as opposed to stellar pulsations or other more stable periodicities,

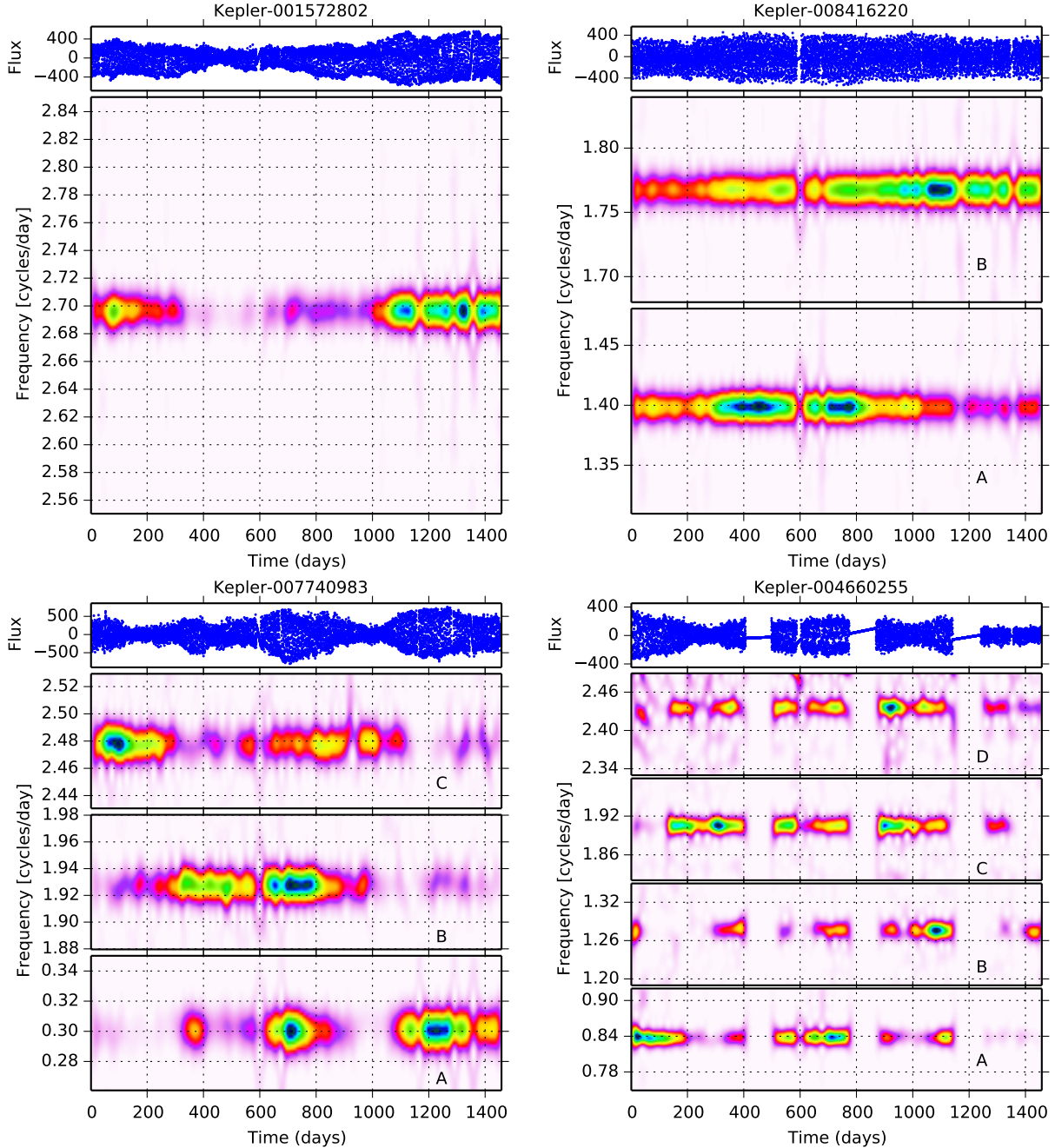


FIG. 5.— Illustrative “sonograms”, or temporally resolved Fourier transforms, of the same *Kepler* M-star targets whose full FTs are shown in Fig. 4. In each quadrant, the upper sub-panel shows the flux time series for the object, while the lower sub-panel is the sonogram. Each periodicity has its own intensity normalization. The color coding is related to the FT amplitude with purple/red through green/blue the lower-to-higher amplitudes, respectively. Note how most of the modulation amplitudes vary strongly with time and independently of one another. These sonograms help demonstrate that the modulations are due to rotating starspots and not binary star modulations or stellar pulsations.

e.g., binary modulations.

5. TRACKING THE MODULATION PHASES

It would not be surprising to find that starspots produce modulations with phases that are quite variable, as are the amplitudes per the above discussion. Therefore, we devised a way to track the phases of the observed periodicities in order to assess their characteristics and determine whether they suggest an origin in starspots. Because the FTs of the inferred rotationally induced spot

modulations have harmonics that fall off rapidly in amplitude with frequency, we model the modulations by just the base frequency and its first harmonic. We can then describe the flux locally in the time series by the expression:

$$\mathcal{F}(t) = A + B \sin(\omega t + \phi_1) + C \sin(2\omega t + \phi_2) \quad (2)$$

where $\omega \equiv 2\pi/P_{\text{rot}}$. For each point in the flux time series, we fit a function of the form given by Eqn. (2) over a short interval of time equal to 2 to 4 base periods

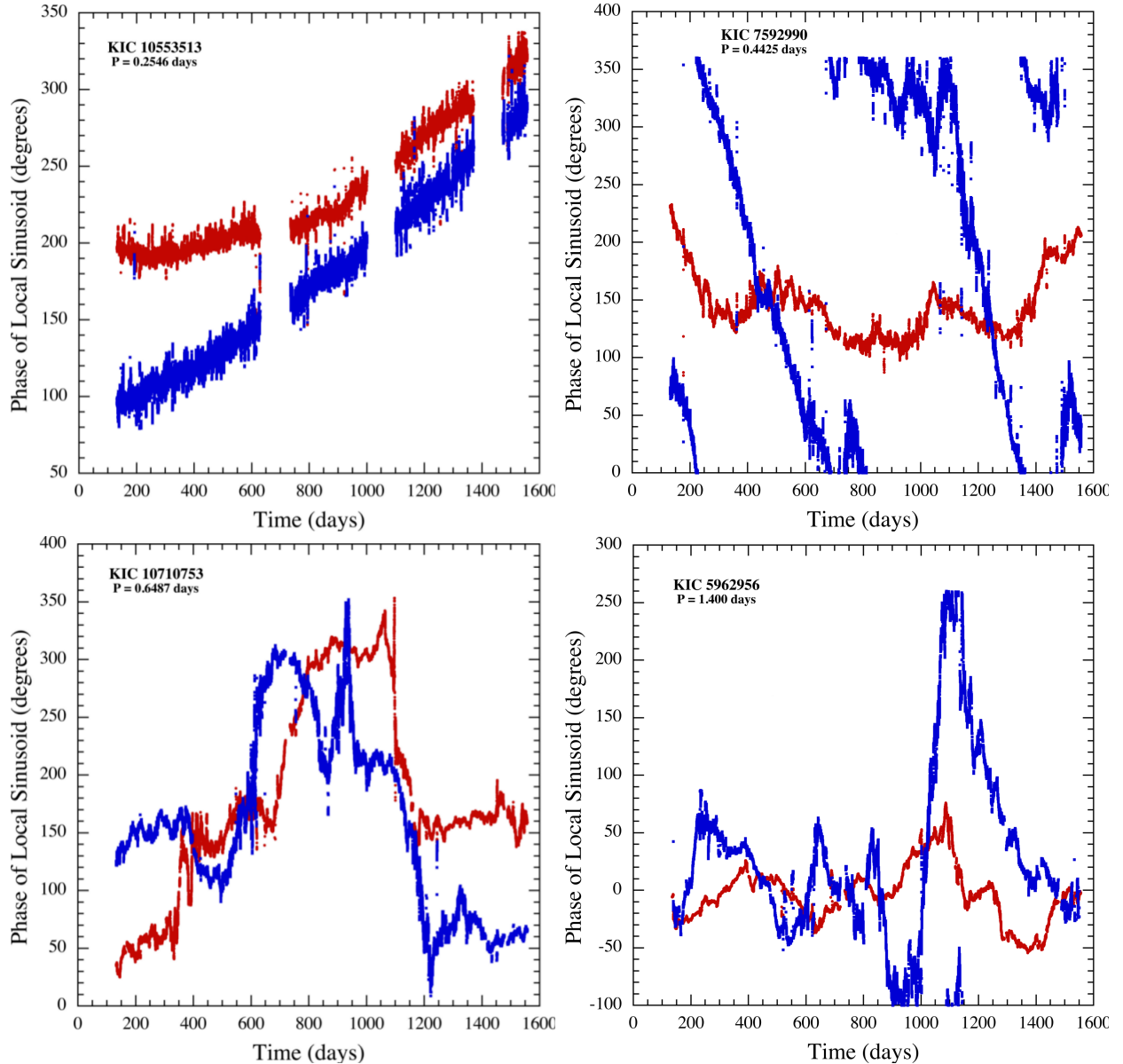


FIG. 6.— Illustrative phase tracking diagrams for four systems that appear to exhibit periodic modulations due to starspot rotations. The inferred rotation periods range from 0.25 days to 1.4 days. The red and blue curves are the fitted values with time of ϕ_1 and ϕ_2 defined in Eqn. (2), which represent the locally defined phase of the base frequency and its first harmonic, respectively. The two phases are typically seen to vary erratically with time, as might be expected for transitory, migrating, and differentially rotating starspots.

of the modulations, depending on the statistical precision that is desired. For periods between 1/4 and 2 days, this corresponds to using between 25 and 400 flux points to determine five unknown parameters, including the phases ϕ_1 and ϕ_2 . The phases of the base frequency and of its first harmonic are thereby computed for every point in the time series.

Results of this ‘phase tracking’ are shown in Fig. 6 for four M-star targets for which we found, in each case, a single rotation period in the range from 0.25 to 1.4 days. The phases of the base frequency are plotted in red points while those of the first harmonic are shown in blue. Portions of the phase curves with linear trends indicate times of constant effective frequency; regions with curvature indicate changes in the apparent frequency. These plots tend to exhibit two different signatures that are likely

characteristic of transitory, migrating, and differentially rotating starspots: (1) erratic phase behavior, and (2) different phase behavior for the base frequency vs. the first harmonic. The stellar pulsators that we have examined with this same phase-tracking code do not behave in this manner.

More quantitatively, the phase of the modulations can be formally defined as

$$\phi(t) = \int (\nu(t) - \nu_0) dt \quad \text{or} \quad \dot{\phi}(t) = \nu(t) - \nu_0 \quad (3)$$

In terms of the period, this can be written as

$$P(t) \simeq P_0 - \dot{\phi}(t) P_0^2 \quad (4)$$

where ν_0 and P_0 are the reference frequency and period, respectively. The characteristic timescale for period

changes, τ , can be expressed in terms of $\ddot{\phi}$ as:

$$\tau \equiv \frac{P}{\dot{P}} \simeq \frac{1}{P_0 \ddot{\phi}} \quad (5)$$

As numerical examples, we note that a change in phase of 1 cycle (360°) over the *Kepler* mission corresponds to $\dot{\phi} \simeq (1500 \text{ d})^{-1}$ which implies, according to Eqn. (4), a difference in period from the reference period of ~ 0.00017 days (for $P_0 = 1/2$ day). In terms of the implications of curvature in the phase curves, a parabolic arc of $1/6$ of a cycle in amplitude occurring over an interval of ± 200 days corresponds to $\ddot{\phi} \simeq 8 \times 10^{-6}$ cycles day $^{-2}$ with a corresponding value of $\tau \simeq 330$ years.

Finally, we note an important property of these “phase curves”. By construction from Eqn. (2), we see that if the second harmonic term is exactly twice the base frequency, then any slopes in the phase curves should bear the relation $\dot{\phi}_2 = 2\dot{\phi}_1$. However we can see examples in Fig. 6 where this is clearly not the case. For KIC 10553513 the two slopes are nearly the same over the final 800 days of observation, while for KIC 7592990 the mean slope of ϕ_2 is substantially larger than twice the mean slope of ϕ_1 . This is a direct indication that the first harmonic does not occur at exactly twice the base frequency (see also Fig. 7). Vida & Oláh (2013) and Vida et al. (2014) find that KIC 7592990 has an activity cycle on the timescale of about 520 days inferred from the systematic change of its rotational period due to differential rotation, with an estimated lower limit of $\alpha = 0.0012$ (see Eqn. 6). In turn, this likely demonstrates that the second harmonic may arise from spots that are located at both different longitudes *and* different latitudes, with the attendant differential rotation when latitude differences are present. Clustering of starspots at two active longitudes opposite to each other, on close binaries of dwarf stars, has been theoretically investigated by Holzwarth & Schüssler (2003), showing that with faster rotation the occurrence of this clustering is higher (but the initial parameters of the rising flux tubes also play a significant role).

6. MULTIPLE PERIOD SYSTEMS

Upon further careful examination of the FTs of the 178 systems with short rotation periods among the *Kepler* M stars, we find ~ 30 objects with two or more incommensurate periods, at least one of which has $P_{\text{rot}} < 1$ day, and a second that has $P_{\text{rot}} < 2$ days. KIC 8416220, discussed above, provides an example of an M star that exhibits two periodicities; see the upper right panel of Fig. 4. Note that the amplitudes of all three visible harmonics at each frequency have very similar amplitudes. The two base frequencies differ by only $\sim 20\%$.

Further scrutiny also reveals several objects with three or more independent short periods, at least one of which has $P_{\text{rot}} < 1$ day. One particular example is KIC 7740983 whose FT is shown in the lower left panel of Fig. 4. The three independent frequencies, labeled “A”, “B”, and “C” exhibit 3, 7, and 11 harmonics, respectively, out to 25 cycles/day.

One of the systems whose FT we studied exhibited *four* independent frequencies: KIC 4660255 (see lower right panel of Fig. 4). All four periods have $P_{\text{rot}} < 1.2$ days.

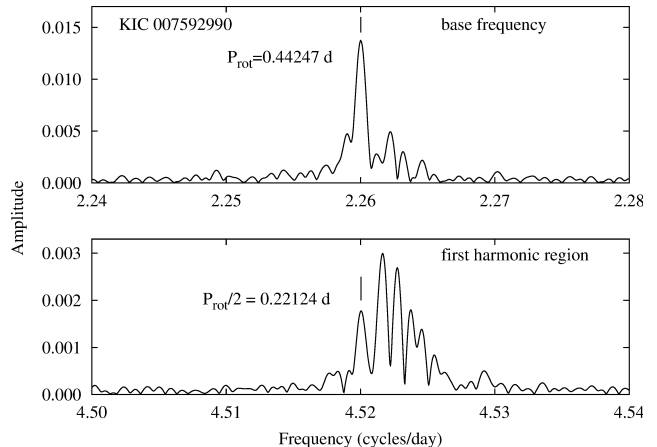


FIG. 7.— Zoom-in on the Fourier transform for KIC 7592990 around the base frequency and its first harmonic. Note that both peaks are broadened well beyond the frequency resolution of the 1500-day *Kepler* data train. The aligned vertical lines in the two panels represent the base frequency and twice the base frequency. As noted in the text, it is evident that the centroid of the first harmonic has a frequency that is clearly higher than twice that of the base frequency. This effect is also demonstrated by the phase plot in Fig. 6 and indicates starspots at different latitudes undergoing differential rotation.

The results of the multiple M-star detections are summarized in Table 2 which lists 37 systems. Of these, 27 have one period with $P_{\text{rot}} < 1$ day, another with $P_{\text{rot}} < 2$ days, and each independent frequency has at least a base frequency plus the next higher harmonic. For 7 of the other systems listed in Table 2, they satisfy all of these criteria, except that one of the periodicities does not have a detectable harmonic. Finally, a few remaining systems have a second period that is slightly longer than 2 days.

7. BINARY AND HIERARCHICAL M-STAR SYSTEMS

We take the presence of two or more periodicities with incommensurate periods, as described in the previous section, as evidence for the presence of two or more rapidly rotating spotted stars within the photometric aperture. This conclusion seems inevitable, since these cases are similar to the cases where only one periodicity is seen in a given target, and since we know of no evidence, for any of these periodicities, that indicates they are due to binary system modulations or stellar pulsations.

A simple statistical argument indicates that most of these targets where two or more periods have been found must consist of multiple physically related stars, i.e., stars in bound systems. Of the approximately 4000 M stars we studied, ~ 200 or $\sim 5\%$ have at least one rotation period shorter than 2 days, and about 100 or $\sim 2.5\%$ have at least one rotation period shorter than 1 day. Thus, given a *Kepler* target that exhibits a periodicity with $P_{\text{rot}} < 1$ day, the probability that a second periodicity with $P_{\text{rot}} < 2$ days will also be apparent is $\sim 5\%$ times the chance that the image of a second M star is in the photometric aperture of the target. The probability of finding two other M stars with $P_{\text{rot}} < 2$ days by chance coincidence in the aperture must be lower than 0.3%. If we have examined 110 objects with $P_{\text{rot}} < 1$ day, we should have found, by chance, *fewer* than 5 and $1/4$ systems with either 2 or 3 M stars, respectively, in the same *Kepler* photometric aperture with $P_{\text{rot}} < 2$ days. The ac-

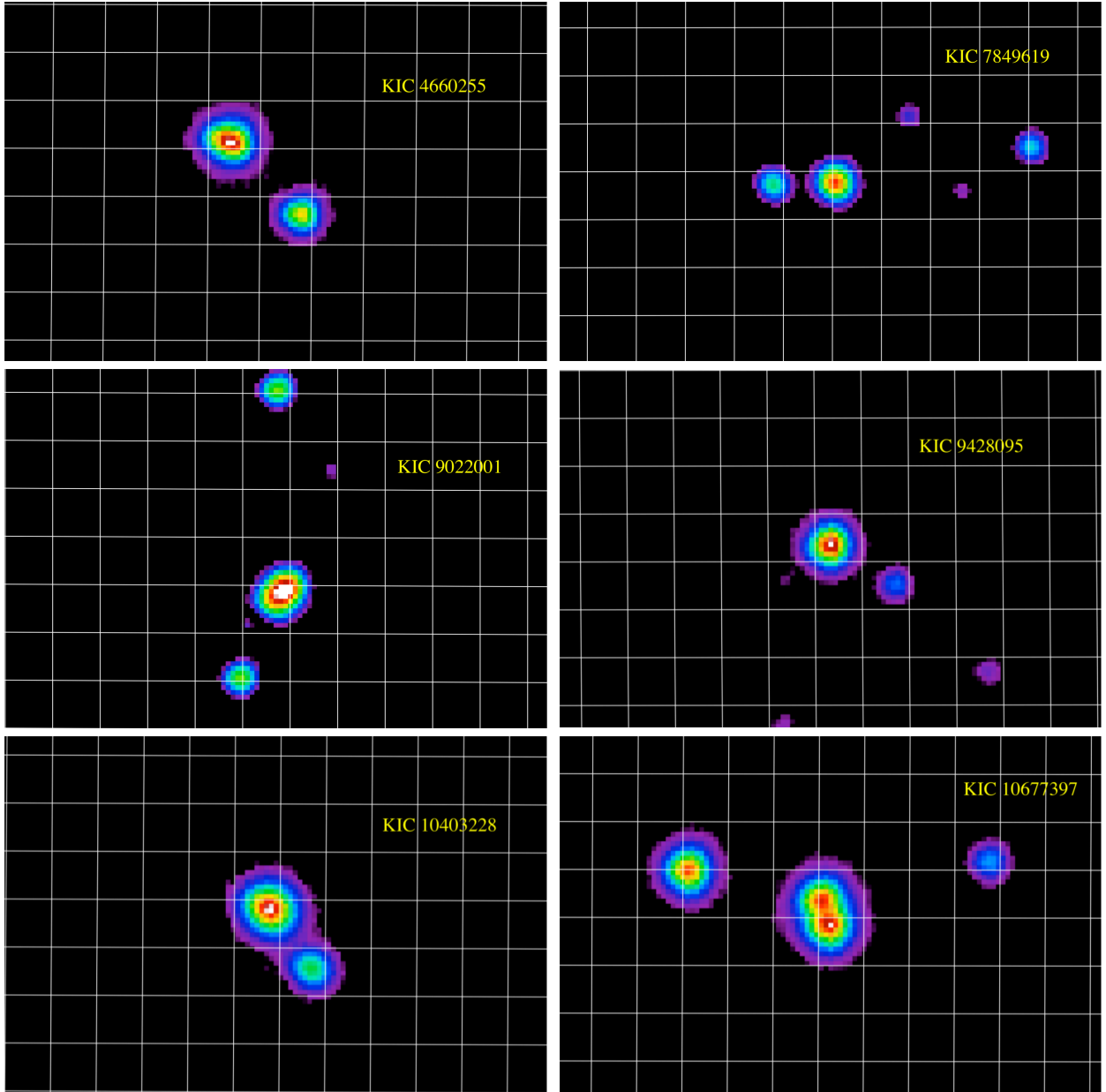


FIG. 8.— Selected set of UKIRT J-band images of *Kepler* M-stars which exhibit multiple rotation periods. North is up and East is to the left. From left to right and then down, they are KIC 4660255, KIC 7849619, KIC 9022001, KIC 9428095, KIC 10403228, and KIC 10677397. The white grid lines are separated by $2'' \times 2''$. In all cases, North is up and East is to the left. The images have been slightly smoothed with a 2D Gaussian with $\sigma = 0.2''$. The color scale is related to the square root of the flux. KIC 7849619, KIC 9428095, and KIC 10403228 appear as fairly close doubles, i.e., with separations of $\sim 2.5'' - 3.0''$. KIC 10677397 has a barely resolved stellar core (separation $\sim 1''$) and has two possible stellar companions at $6''$ and $7''$. KIC 9022001 and KIC 4660255 are apparent doubles separated by $\sim 4''$, and, in each case, the brighter star is elongated and may itself be a binary.

tual values are 30 and 3 (see Table 2), both significantly in excess of what could be expected by chance. Here we have implicitly assumed that, on average, there is much less than one serendipitously occurring second or third detectable M star in any given photometric aperture.

In the above discussion and probability estimates for finding two or more rapidly rotating stars within the same *Kepler* photometric aperture, we made the assumption that the second and third stars were also M stars. If we loosen that assumption, then we can draw on the broader statistics about rotation periods in the *Kepler* sample found by Reinhold, Reiner, & Basri (2013). They

identified periodic variations presumably due to spots on rotating stars, and thereby compiled the rotation periods of all active *Kepler* stars. Out of their sample of 21,100 stars, they found 925 with periods $\lesssim 2$ days. Thus, rapidly rotating stars comprise only 4.5% of stars across the spectral types studied by *Kepler*. This is essentially the same value as we found for our M-star sample, and thus the statistical argument presented above is again applicable, i.e., there is a rather low probability of finding additional rapidly rotating active stars with any of a range of spectral types in the same aperture as the first M star with a short period.

We therefore adopt the working hypothesis that each M star target having a detected periodicity with $P_{\text{rot}} < 1$ day and also one or more additional incommensurate rotational periodicities with $P_{\text{rot}} < 2$, must actually consist of multiple M stars bound in a single system.

Finally, we note that 12 of the 37 systems listed in Table 2 have two short periods that are similar, i.e., they differ by no more than 4% to 25%. There is one system where two periods differ by only 1%. This phenomenon can have two explanations. The first is that the two periods originate in an M-star binary with two nearly equal mass stars of essentially the same age and spin-down history. Thus, perhaps the closeness of a pair of rotation frequencies is not at all unexpected.

The second possibility would be that two close periods come from spots at different latitudes of a single star that is undergoing differential rotation. Reinhold et al. (2013) have carried out an extensive study of differential rotation in 40,660 active *Kepler* stars. In some 18,600 of these stars they find two or more close rotation periods which they take as evidence of differential rotation and which they then use to derive limits on the differential rotation properties. Their Fig. 15 summarizes the measured horizontal shear differential rotation parameter $\Delta\Omega$, which is defined as the difference in rotation frequency between the equator and the pole. For stars hotter than ~ 6000 K, values of $\Delta\Omega$ are often found to exceed 0.2 rad d^{-1} . However, for cool stars, of the type we are studying here, $\Delta\Omega$ averages about 0.07 rad d^{-1} and only rarely exceeds 0.1 rad d^{-1} . We translate this to a fractional differential rotation parameter, α , for cool stars of arbitrary rotation rate:

$$\alpha \equiv \frac{\Delta\Omega}{\Omega_{\text{eq}}} \simeq 0.01 P(\text{days}), \quad (6)$$

where Ω_{eq} is the equatorial rotation frequency of the star, and $P = 2\pi/\Omega_{\text{eq}}$. If this relation indeed holds down to short periods (e.g., 1/2 day), then it implies that any two short periods we detect which are different by more than a few percent are *not* likely due to differential rotation.

In any event, the possibility that some of the periodicities we see may arise on the *same* star should be kept in mind, though we do not expect this to be the situation in many cases. Future tests with high resolution AO imaging and ground-based spectroscopy can be of further help for checking this possibility.

Reinhold et al. (2013) also show (in their Fig. 8) that there is a strong trend for stars that are of spectral type F and earlier to rotate more rapidly than cooler stars which are presumably braked by magnetically constrained stellar winds (see, e.g., Mestel 1968; Skumanich 1972; Smith 1979; Zwaan 1981; Verbunt & Zwaan 1981). Such magnetic braking likely requires dynamo activity that is stronger in stars with convective envelopes. Therefore, according to Barnes & Sofia (1996) and Barnes (2007), M stars that are rotating with periods shorter than 2 days are probably relatively young, i.e., \lesssim one to a few hundred Myr (see also Sect. 10).

An alternative to the “youth hypothesis” is that the short periods we see are indeed due to spots on rotating stars, but in tidally locked close binaries. One such example is V405 And with active components consisting of M0V+M5V spectral types and rotational/orbital periods

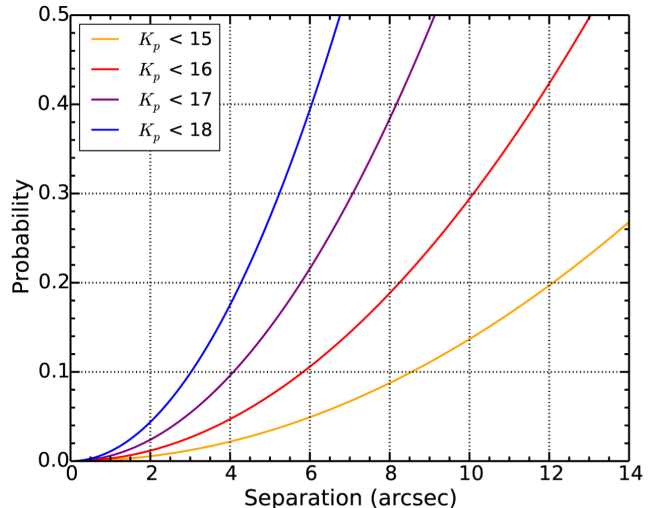


FIG. 9.— Probability of chance alignment of background or foreground stars with our *Kepler* M-star target, brighter than the indicated magnitude, as a function of separation.

of 0.465 day (Vida et al. 2009). Since the light curves of our short period systems do not exhibit obvious eclipses or ellipsoidal light variations¹¹, this would imply that we are viewing the systems at small orbital inclination angles. However, that would make the situation even more extreme in the sense that each such short period would itself require a binary. Thus, in systems where we see three or four short periods, this hypothesis would require 6-8 bound stars, which is rather implausible.

8. IMAGING EVIDENCE FOR MULTIPLICITY

8.1. UKIRT Images

We have inspected the UKIRT J-band images¹² for the 37 systems listed in Table 2 which exhibit two to four rotation periods. In general, for the UKIRT images of the *Kepler* field, one can easily distinguish two stars of comparable brightness that are separated by $\gtrsim 1.5''$, while for objects separated by less than $\approx 1''$, there is a single image. Often, it is possible to discern that the image is elongated for stellar separations as small as $\approx 0.5''$. Nineteen of the UKIRT J-band frames appear to show single stellar images. However, 11 show an apparent companion, or more than one companion, with a separation of $\lesssim 5''$, while 7 of these have separations $\lesssim 3''$. Thus, there is tentative evidence for multiplicity in the UKIRT images of $\approx 30\%$ of the systems in Table 2.

In reviewing the evidence, it is good to keep in mind that a separation of $1''$ at typical distances of ~ 200 pc corresponds to a physical separation of 200 AU. If, for sake of argument, bound stellar pairs are taken to have orbital separations between 0.01 AU and 10^5 AU that are distributed uniformly in terms of the logarithms of the separations (e.g., Dhital et al. 2010), then fewer than half of them will have orbital separations $\gtrsim 200$ AU. Thus, the UKIRT image multiplicity numbers noted above do

¹¹ In ellipsoidal variations the main peak in the FT occurs at twice the orbital frequency, 2ν , with very small contributions at ν , and 3ν . We see no such cases. There is also the possibility that the amplitudes at ν and 3ν are too low to be detected, leaving only the peak at 2ν . Several cases of frequencies with no other harmonics are indeed seen, but these are clearly marked in Table 2.

¹² <http://keplerscience.arc.nasa.gov/ToolsUKIRT.shtm1>

not rule out the possibility that all of the 37 multiple M-star candidates are in bound hierarchical systems (see e.g., Sect. 8.2 for some examples of closer pairs).

In Fig. 8 we present six examples of multiple M-star candidates that show direct evidence for multiple stellar images within the *Kepler* photometric aperture. These systems are: KIC 4660255, 7849619, 9022001, 9428095, 10403228, and 10677397, and they are included in Table 2 along with their periods. The *Kepler* magnitudes of these stars range from 15.3-16.1. The magnitudes and densities of stellar images in Fig. 8 indicate that most of these pairs of images are likely to be physically related as opposed to chance alignments. In Fig. 9 we show the probability of interlopers (i.e., background or foreground stars) coming within a given angular distance of any particular *Kepler* target star. These estimates were obtained by calculating a uniform stellar density from the 10th release of the *Kepler* Input Catalog (KIC10)¹³ for a given magnitude limit within a 115 square degree field of view (Borucki et al. 2010). The mean stellar densities are likely slight overestimates since the KIC10 catalog includes roughly 36,000 calibration stars outside the *Kepler* field of view. Although the stellar density is not uniform over *Kepler*'s field of view—rather it varies with Galactic latitude—the distribution of our multi-period sources are uniform in Galactic latitude supporting our conclusion that the multi-period sources are most likely bound companions rather than interlopers. We can see from Fig. 9 that for stars comparable to, or up to 1-2 magnitudes fainter than, our $K_p = 15$ -16 magnitude target M stars, it is worth considering stars out to $\sim 5''$ as possibly physically related to the M star in question.

The white grid lines in Fig. 8 are drawn with a spacing of $2'' \times 2''$. The images have been slightly smoothed with a 2D Gaussian with $\sigma = 0.2''$. KIC 7849619, KIC 9428095, and KIC 10403228 appear as fairly close doubles with separations of $\sim 2.5'' - 3.0''$. KIC 10677397 has a barely resolved stellar core (separation $\sim 1''$) and has two possible stellar companions at $6''$ and $7''$. KIC 9022001 and KIC 4660255 are apparent doubles separated by $\sim 4''$, and, in each case, the brighter star is elongated and may itself be a binary. Finally, we remind the reader that KIC 4660255 is the remarkable object that exhibits four independent periods, all < 1.2 days. This target is discussed in detail in Section 9.

Some of these separations seen in the UKIRT images are sufficiently large, i.e., $2'' - 5''$, that the point-spread-function (“PSF”) fitting technique (Still & Barclay 2013) may be useful for identifying which of the stellar images is the source of a particular periodicity. This method is applied to KIC 4660255 in Section 9.

8.2. Keck AO Images

Images of four targets in our sample were obtained with the NIRC2 camera using the Keck II adaptive optics (AO) system during the past ground-based observing season for the *Kepler* field. We observed KIC 4175707, KIC 11955208, and KIC 8416220 on 2013 May 30 (UT) using the laser guide star to close the AO system control loops (Wizinowich et al. 2006). The targets were imaged in K' at low air mass ($\sec z < 1.1$) using a 3-point dither pattern with $2''$ dither spacings. Three images

were obtained at each dither position with integration times of 2, 3, and 2 s incorporating 10, 5, and 10 coadds per frame for a total integration time per target of 180, 135, and 180 s, respectively. KIC 7740983 was imaged on the night of 2013 August 18 with Keck II/NIRC2 natural guide star AO (Wizinowich et al. 2000) in the K_s band. The same 3-point dither was performed for this target with 3-s integrations, and 10 coadds per frame for a total integration time of 180 s.

Each dither frame was corrected for bad pixels, sky subtracted, and flat fielded. Centroids were obtained by fitting the core of the Airy pattern with a two dimensional Gaussian function. The final images in Figure 10 show the medians of the aligned dither stacks for each target.

Each of these four targets shows a pair of rotation periods (in days) that are shorter than 1 day, viz., $\{0.57, 0.72\}$, $\{0.40, 0.52\}$, $\{0.56, 0.70\}$, and $\{0.34, 0.42\}$, for KIC 8416220, KIC 7740983, KIC 11955208, and KIC 4175707, respectively. Amazingly, three of the four systems show close twin pairs of M stars in what are almost certainly bound binaries if not higher-order multiples. Only KIC 4175707 still appears single at the $0.05''$ level.

9. SPECIAL CASE OF KIC 4660255

In this section we examine KIC 4660255, which exhibits four rotational periodicities all with periods shorter than 1.2 days. As the upper left panel of Fig. 8 shows, at the location of KIC 4660255 there are two point-like images that are separated by $4.2''$, and, hence, are well within the photometric aperture. Still & Barclay (2014) have devised a point-spread function (“PSF”) fitting technique that can utilize data at the pixel level to compute light curves for each of several stars within the photometric aperture. In brief, we assume here that the two stars can be characterized as two point-spread-functions with two unknown fluxes and shifts of the photometric aperture relative to the sky, $\Delta\alpha$ and $\Delta\delta$ (see Fig. 11). We then minimize upon the uncertainty-weighted residuals between the pixel-level data and the fit in order to yield the flux and pixel position of both stars for every one of 48,100 exposures across quarters Q1-16. This technique was demonstrated in the case of KOI 2700 to determine which of two stars within the photometric aperture was the source of planet transits (Rappaport et al. 2013).

We have carried out a PSF analysis for KIC 4660255 to try to identify from which of the two well-separated images (see Fig. 8) the various rotation frequencies arise. We show in Fig. 11 an example of a single frame of pixel-level data for this object. The upper left panel shows the $4'' \times 4''$ *Kepler* pixels within the pixel mask for KIC 4660255 for a single frame of the 50,575 available for this object. The best fitting PSF model, comprised of two stars, is shown in the upper right panel. When this model is integrated over the pixels, the “fit” is shown in the lower left panel. The residuals with respect to the data from that frame, are shown in the lower-right panel. This process was repeated for each of the 50,575 frames for KIC 4660255, thereby yielding two photometric time series, one for each star.

The resultant FTs for the time series extracted from the two stars within the aperture of KIC 4660255 are shown in Fig. 12. The top panel shows the FT for the

¹³ <https://archive.stsci.edu/kepler/kic10/search.php>.

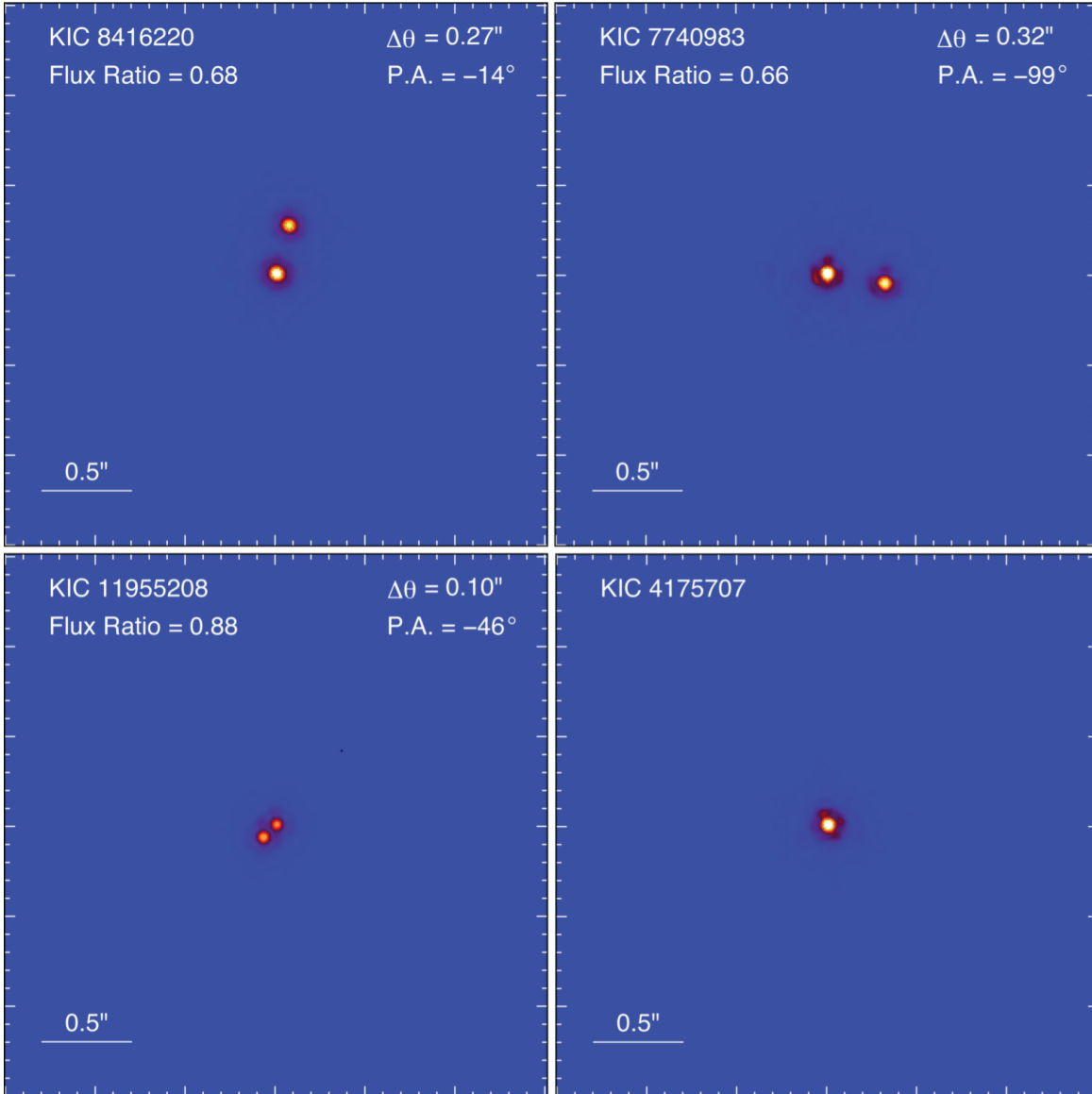


FIG. 10.— Keck adaptive optics images for four of our candidate multiple M-star systems. North is up and East is to the left. KIC 8416220, 11955208, 4175707 were recorded at K' band, while the image of 7740983 was taken in the K_s band. All except KIC 4175707 are obvious close twin binary M stars. The angular separations between components ranges between $0.1''$ and $0.32''$, corresponding to physical separations of ~ 20 -65 AU at nominal distances of 200 pc. Flux ratios and position angles of the two components in degrees East of North are displayed where applicable.

brighter of the two stars (the more northerly one). Only the A and B frequencies are present at a detectable level. The corresponding periods are 1.1958 days and 0.7859 days. No evidence is seen for the shorter C and D periods. In contrast, the bottom panel in Fig. 12 shows the C and D periods, 0.5251 and 0.4108 days, very clearly. In addition, the first two harmonics of the A periodicity leak through weakly – at about $1/5$ of the amplitude that they exhibit in the upper panel. Thus, the PSF fitting technique appears to have cleanly distinguished the four periodicities as being from two different stellar sources. In turn, we can marginally discern from Fig. 8 that the northerly image which is host to periods A and B likely comprises two images, and we propose that each of those is the source of one of the A and B periods. By analogy, we hypothesize that the fainter, more southerly image is

itself a binary, each star of which is rotating with the C or D period.

10. SUMMARY AND CONCLUSIONS

In this work we have searched the *Kepler* photometric data base of M stars for short rotation periods. We found 178 *Kepler* targets with 211 different periods of $P_{\text{rot}} < 2$ days and 110 systems with 127 different periods with $P_{\text{rot}} < 1$ day. Some 30 of these objects exhibit two or more rotation periods where at least one has $P_{\text{rot}} < 1$ day and the other has $P_{\text{rot}} < 2$ days. We also find several systems with three or more rotation periods where at least one has $P_{\text{rot}} < 1$ day and the others have $P_{\text{rot}} < 2$ day. There are a sufficient number of these with more than one short rotation period to allow us to argue that they are likely young, physically related, binary or hierarchical triple systems.

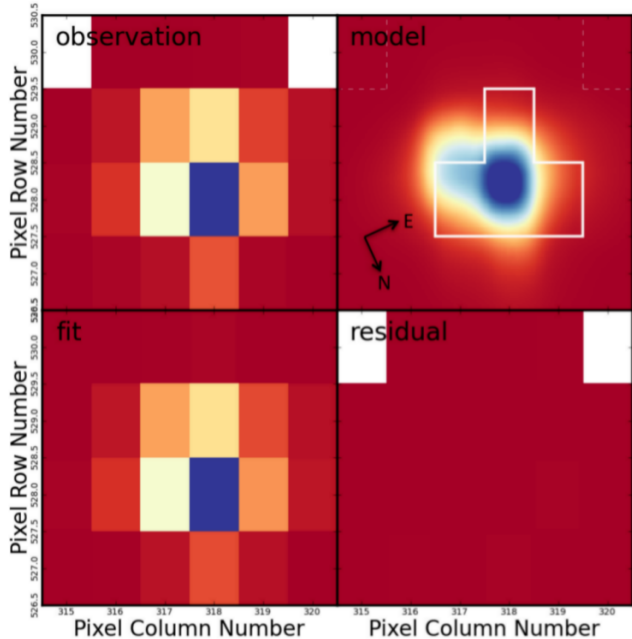


FIG. 11.— Typical 29.4-min. long-cadence observation of KIC 4660255, at the pixel level (each pixel is $4'' \times 4''$), for one particular frame of $\sim 50,000$ exposures. The pixel mask for KIC 4660255 contains at least two stars – the bright blue pixel at $\{318, 528\}$ as well as a fainter companion star that is about $4''$ to the left (see Fig. 8). The best PSF model fit is plotted in the top-right, while that fit, rebinned across the detector pixels, is compared at the lower-left. The lower-right panel contains the residuals between the data and the best fit. All images are plotted on a linear intensity scale. PSF-derived light curves are constructed by repeating this fit for every exposure over quarters 1 to 16. The objective is to disentangle the fluxes between the two stars within the pixel mask. The approximate orientation of the pixels with respect to the sky is indicated by the compass in the upper right panel. The inverted “T”-shaped region in the same panel indicates a typical pixel-level photometric aperture for this target used for conventional analyses.

At least 6, and perhaps as many as 14, of these M-star systems show, in the UKIRT *Kepler* region survey J-band images, multiple stellar images¹⁴ that may represent physically related stars. Three more systems were clearly resolved in Keck AO images of four systems. These are almost certainly physically bound twin M-star binaries. It seems quite likely that additional AO imaging in the future will reveal that more of these 30 multiple-period systems contain multiple stellar images. Spectroscopy could further reveal closer binary members.

If most of these M-star systems with multiple short periods indeed turn out to be multiple bound M-stars, this could prove a valuable way of discovering young hierarchical M-star systems. We suggest that this approach may also be applicable to K and G stars.

In the process of conducting this study we found that approximately 5% of all M stars are rotating with periods shorter than 2 days. If we utilize standard models of contraction onto the main sequence, with the consequent *spinup* of the star due to conservation of angular momentum, and the loss of systemic angular momentum due to magnetic braking (see, e.g., Kawaler 1988; Chaboyer et al. 1995; Barnes & Sofia 1996; Irwin et al. 2011) we can check whether M stars spend sufficient time rotating

¹⁴ These 14 systems are ones with another stellar image within $\sim 5''$ of the target and within $\sim |\Delta J| \lesssim 2$.

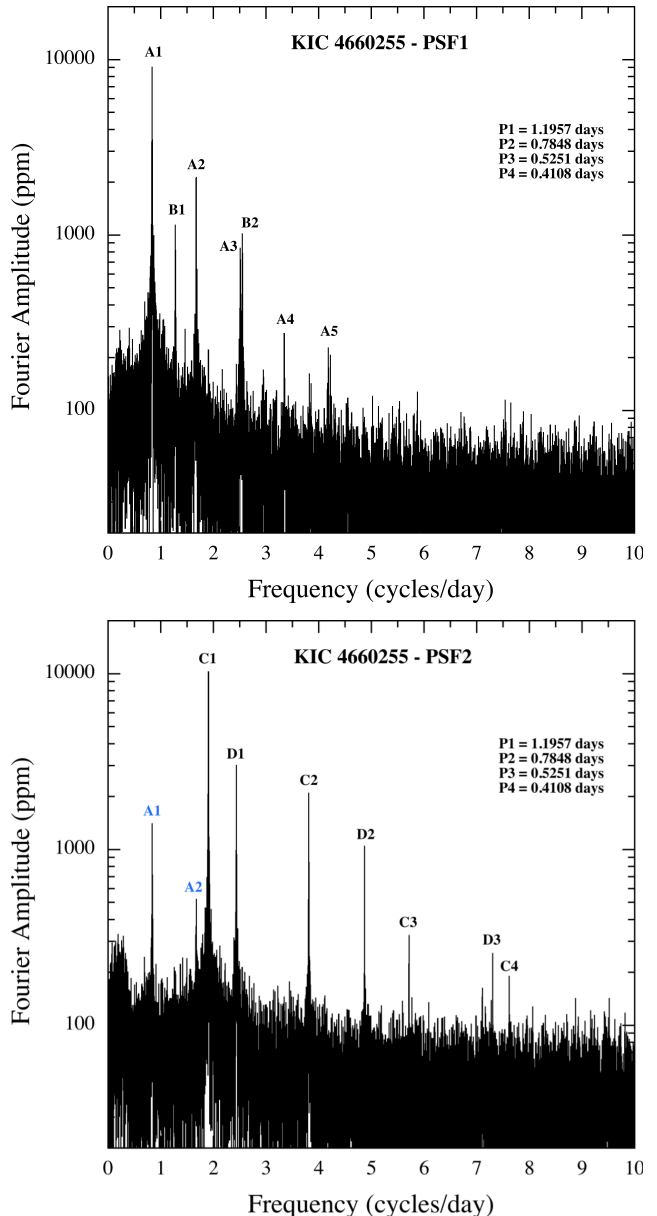


FIG. 12.— Fourier transforms of the PSF analyzed data trains for KIC 4660255. Top: This is the PSF-extracted data train for the brighter of the two stars within the pixel mask. Note that of the four periodicities in this *Kepler* target, only the longer two periods show up clearly. Bottom: PSF-extracted data train for the fainter of the two stars within the pixel mask. Here, the shorter two periods show up prominently, with only a small “leakage” of the brighter star and its period of 1.19 days. Thus, we associate two rotation periods with the brighter star and the other two with the fainter star.

rapidly to allow for 5% of them to have $P_{\text{rot}} \lesssim 2$ days. These models typically take the magnetic braking torque to be proportional to ω_{rot}^3 when $\omega_{\text{rot}} < \omega_{\text{sat}}$, where ω_{sat} is a “saturation” frequency, above which the torque is proportional to $\omega_{\text{rot}} \omega_{\text{sat}}^2$. As an example of a model spin history of an M star, see Fig. 13 of Irwin et al. (2011; dashed curve). We see that a minimum rotation period of 0.3 days is attained at ~ 10 Myr, and the period lengthens to more than 1 day at 300 Myr and 2 days at 400 Myr. Thus, at least for this specific example, which involves numerous uncertainties, the fraction of time that

a 10^{10} year old M star has spent with $P_{\text{rot}} \lesssim 2$ days is about 4% of its lifetime. This is reassuringly consistent with the fraction of M stars that we find are rotating rapidly.

We acknowledge several useful discussions about the particular M star(s) KIC 7740983 with Robert Szabo and Katrien Kolenberg. We also thank Cristina Rodriguez-Lopez, Jim MacDonald, Jérôme Quintin, Alex Brown, Günter Houdek, and Lucianne Walkowicz for important discussions about the possibility of observing M-star pulsations with *Kepler*. Arthur Delarue wrote a very helpful code for automatically extracting significant incommensurate frequencies from Fourier transforms. We thank Sasha Hinkley and Benjamin Montet for performing a subset of our Keck AO observations. We are grateful to the *Kepler* team for providing such valuable data to the community. D.H. acknowledges NASA support through the Kepler Participating Scientist Program under Grant NNX14AB92G. R.S.O. acknowledges support through the Kepler Participating Scientist Program and the NASA Origins Program under Grants NNX12AC76G and NNX11AG85G. P.S.M. acknowledges support from the Hubble Fellowship Program, provided by NASA through Hubble Fellowship

grant HST-HF-51326.01-A awarded by the STScI, which is operated by the AURA, Inc., for NASA, under contract NAS 5-26555. G.H. is grateful for support by the Polish NCN grant 2011/01/B/ST9/05448. K.O. and K.V. acknowledge support from the Hungarian OTKA grants K-81421 and K-109276, and from “Lendület-2012” Young Researchers’ Programs of the Hungarian Academy of Sciences. This research has made use of the NASA Exoplanet Archive, and the Mikulski Archive for Space Telescopes (MAST). We made use of J-band images that were obtained with the United Kingdom Infrared Telescope (UKIRT) which is operated by the Joint Astronomy Centre on behalf of the Science and Technology Facilities Council of the U.K. Some of the data presented herein were obtained at the W.M. Keck Observatory, which is operated as a scientific partnership among the California Institute of Technology, the University of California and the National Aeronautics and Space Administration. The Observatory was made possible by the generous financial support of the W.M. Keck Foundation. We acknowledge the very significant cultural role and reverence that the summit of Mauna Kea has always had within the indigenous Hawaiian community, and we are most fortunate to have the opportunity to conduct observations from this mountain.

REFERENCES

- Baraffe, I., Chabrier, G., Allard, F., & Hauschildt, P.H. 2002, *A&A*, 382, 563
- Barban, C., Beuret, M., Baudin, F., Goupil, M.-J., Samadi, R. 2013, *J. Phys. Conf. Ser.*, 440, 012031
- Barnes, S., & Sofia, S. 1996, *ApJ*, 462, 746
- Barnes, S.A. 2007, *ApJ*, 669, 1167
- Batalha, N.M., Borucki, W.J., Koch, D.G. et al. 2010, *ApJ*, 713, 109
- Batalha, N. M., Borucki, W. J., Bryson, S. T., et al. 2011, *ApJ*, 729, 27
- Batalha, N.M., Rowe, J.F., Bryson, S.T., et al. 2013, *ApJS*, 204, 24
- Bedding, T. 2011, arXiv:1107.1723
- Birkby, J., Nefs, B., Hodgkin, S., et al. 2012, *MNRAS.*, 426, 1507
- Borucki, W.J., Koch, D., Basri, G., et al. 2010, *Sci*, 327, 977
- Borucki, W.J., Koch, D.G., Basri, G. 2011, *ApJ*, 736, 19
- Boyajian, T.S., von Braun, K., van Belle, G., et al. 2012, *ApJ*, 757, 112
- Brown, T.M., Gilliland, R.L., Noyes, R.W., et al. 1991, *ApJ*, 368, 599
- Brown, T.M., Latham, D.W., Everett, M.E., & Esquerdo, G.A. 2011, *AJ*, 142, 112
- Bryson, S. T., Jenkins, J. M., Gilliland, R. L., et al. 2013, arXiv:1303.0052
- Burke, C.J., Bryson, S.T., Mullally, F., et al. 2013, submitted to *ApJ*, arXiv: 1312.5358
- Chaboyer, B., Demarque, P., & Pinsonneault, M. H. 1995, *ApJ*, 441, 865
- Chabrier, G. 2003, *PASP*, 115, 763
- Collier Cameron, A. 2007, 328, 1030
- Corsaro, E., Fröhlich, H.E., Bonnano, A., et al. 2013, *MNRAS*, 430, 2313
- Cruz, K.L., & Reid, I.N. 2002, *AJ*, 123, 2828
- Delfosse, X., Forveille, T., Perrier, C., & Mayor, M. 1998, *A&A*, 331, 581
- Dhital, S., West, A.A., Stassun, K.G., & Bochanski, J.J. 2010, *AJ*, 139, 2566
- Dressing, C.D., & Charbonneau, D. 2013, *ApJ*, 767, 95
- Duchêne, G. & Kraus, A. 2013, *ARA&A*, 51, 269
- Henry, T.J., Kirkpatrick, J.D., & Simons, D.A. 1994, *AJ*, 108, 1437
- Henry, T.J., Jao, W.-C., Subasavage, J.P., Beaulieu, T.D., Ianna, P.A., Costa, E., & Méndez, R.A. 2006, *ApJ*, 132, 2360
- Holzwarth, V. & Schüssler, M. 2003, *A&A*, 405, 303
- Irwin, J., Berta, Z.K., Burke, C.J., Charbonneau, D., Nutzman, P., West, A.A., & Falco, E.E. 2011, *ApJ*, 727, 56
- Jenkins, J. M., Borucki, W. J., Koch, D. G., et al. 2010, *ApJ*, 724, 1108
- Kawaler, S. D. 1998, *ApJ*, 333, 236
- Kjeldsen, H. & Bedding, T.R. 1995, *A&A*, 293, 87
- Koch, D.G., Borucki, W., Basri, G. et al. 2010, *ApJ*, 713, L79
- Kolláth, Z., Oláh, K. 2009, *A&A* 501, 695
- Küker, M. & Rüdiger, G. 2011, *AN*, 332, 933
- Lee, Y.-W., Ree, C. H., Lejeune, T., & Barnes, S. 2001, *ApJS*, 136, 417
- Lissauer, J. J., Marcy, G. W., Rowe, J. F., et al. 2012, *ApJ*, 750, 112
- Mann, A.W., Gaidos, E., Lépine, S., & Hilton, E.J. 2012, 753, 90
- Mann, A.W., Gaidos, E., Kraus, A., & Hilton, E.J. 2013, submitted to *ApJ*, arXiv:1304.7269
- Marcus, R.A., Sasselov, D., Hernquist, L., & Stewart, S.T. 2010, *ApJ*, 712, L73
- Matijević, G., Prša, A., Orosz, J.A., Welsh, W.F., Bloemen, S., & Barclay, T. 2012, *AJ*, 143, 123
- McQuillan, A., Aigrain, S., & Mazeh, T. 2013, *MNRAS*, 432, 1203
- Mestel, L. 1968, *MNRAS*, 138, 359.
- Morton, T.D., & Swift, J.J. 2013, arXiv: 1303.3013
- Muirhead, P.S., Hamren, K., Schlawin, E., Rojas-Ayala, B., Covey, K.R., & Lloyd, J.P. 2012, *ApJ*, 750, L37
- Muirhead, P. S., Johnson, J. A., Apps, K., et al. 2012, *ApJ*, 747, 144
- Oláh, K., Jurcsik, J., Strassmeier, K.G. 2003, *A&A* 410, 685
- Rappaport, S., Barclay, T., DeVore, J., Rowe, J., Sanchis-Ojeda, R., & Still, M. 2014, *ApJ*, 784, 40
- Reid, R.I., Gizis, J.E., & Hawley, S.L. 2002, *AJ*, 124, 2721
- Reiners, A. 2006, *A&A*, 446, 267
- Reinhold, T., Reiners, A., & Basri, G. 2013, *A&A*, 560, 4
- Rodríguez-López, C., MacDonald, J., & Moya, A. 2012, *MNRAS*, 419, 44
- Rodríguez-López, C., MacDonald, J., Amado, P.J., Moya, A., & Mullan D. 2013, *MNRAS*.tmp.2985; arXiv: 1312.2743
- Sanchis-Ojeda, R., Rappaport, S., Winn, J.N., Levine, A., Kotson, M.C., Latham, D. & Buchhave, L. A. 2013, *ApJ*, 774, 54
- Shulyak, D., Seifahrt, A., Reiners, A., Kochukhov, O. & Piskunov, N. 2013, submitted to *MNRAS*, arXiv: 1108.3465
- Skumanich, A. 1972, *ApJ*, 171, 565

- Sotin, C., Grasset, O., & Mocquet, A. 2007, *Icar*, 191, 337
- Smith, M.A. 1979, *PASP*, 91, 737
- Smith, J. C., Stumpe, M. C., Van Cleve, J. E., et al. 2012, *PASP*, 124, 1000
- Still M., & Barclay T., 2013, in preparation
- Stumpe, M. C., Smith, J. C., Van Cleve, J. E., et al. 2012, *PASP*, 124, 985
- Swift, J. J., Johnson, J. A., Morton, T. D., et al. 2013, *ApJ*, 764, 105
- Torres, G., & Giménez, A. 2010, *A&ARv*, 18, 67
- Tran, K., Levine, A., Rappaport, S., Borkovits, T., Csizmadia, Sz., & Kalomeni, B. 2013, *ApJ*, 774, 81
- Verbunt, F., & Zwaan, C. 1981, *A&A*, 100, L7
- Vida, K., Oláh, K., Kóvári, Zs., Korhonen, H., Bartus, J., Hurta, Zs., Posztobányi, K. 2009, *A&A* 504, 1021
- Vida, K. & Oláh, K. 2013, eprint arXiv:1308.2641
- Vida, K., Oláh, K., & Szabó, R. 2014, *MNRAS*, in press (arXiv:1404.4359)
- Wizinowich, P., Acton, D. S., Shelton, A.H. 2000, *PASP*, 112, 315
- Wizinowich, P.L., Le Mignant, D., Bouchez, C. 2006, *PASP*, 118, 297
- Zwaan, C. 1981, in *Solar Phenomena in Stars and Stellar Systems*, eds. R.M. Bonnet & A.K. Dupree (D. Reidel; Dordrecht), p. 463.

TABLE 1
Kepler M STARS EXHIBITING A SHORT ROTATION PERIOD

KIC	Period	KIC	Period	KIC	Period	KIC	Period
1572802	0.3711	6592335	0.4119	8565914	1.4183	10790812	1.0629
2300039	1.7083	6664639	1.4482	8611876	1.5797	10790838	0.9173
2449101	0.7399	6715960	0.9185	8672278	1.8549	10796551	1.1485
2557669	1.8595	6752578	0.2601	8673358	1.0292	10803430	1.5207
3130391	1.2301	6762389	0.3855	8681527	0.5775	10975238	1.9487
3439791	0.4321	6928206	1.2839	8873575	0.6702	11031746	1.2109
3454793	0.6682	6936046	0.5274	8909833	1.2812	11042875	1.5658
3642335	0.6725	6949412	1.6453	8935942	1.6582	11091336	1.1947
3732401	1.7990	7110077	0.9717	9022001	0.6989	11124203	0.9596
3748172	1.0516	7269729	0.3346	9041966	0.1477	11140425	1.1879
3757251	0.2158	7431659	1.0507	9075708	0.5131	11147271	1.8794
3831911	0.5621	7434110	0.4014	9083354	1.1341	11189348	0.5060
3935499	0.9214	7445605	1.0782	9091897	0.2399	11305240	0.7808
3962433	0.4025	7448057	0.3873	9142641	1.3747	11343461	1.6167
4036313	1.5816	7449695	0.5610	9142714	1.1285	11349556	1.6941
4077867	0.4777	7547969	0.6802	9205855	0.9144	11390683	1.1295
4246255	1.3177	7592990	0.4426	9268481	0.5802	11446073	1.0393
4264634	0.7541	7678417	0.6267	9335198	0.2898	11447564	0.3812
4473355	0.2060	7686474	1.4843	9395840	1.0973	11498106	0.5708
4545041	0.3326	7733540	1.5488	9479539	1.8576	11521274	0.6653
4660255	0.4109	7740983	0.4036	9519275	0.5797	11605209	1.8622
4951466	0.1349	7741987	1.2612	9590249	0.2642	11668095	0.9156
5083330	1.9550	7743830	0.3749	9702550	1.6270	11702167	0.3798
5095098	0.7414	7800087	0.4722	9705079	0.5377	11722217	0.1643
5182822	0.3391	7847566	0.3806	9761113	0.6806	11760021	0.7565
5184487	1.1051	7849619	0.3092	9784820	1.1005	11855334	0.8173
5341666	0.3631	7973675	0.4572	9899900	0.4145	11855853	1.4325
5360129	1.3519	8012943	0.5726	9933464	1.2234	11876220	1.4600
5435958	0.8370	8057610	1.7332	9992083	0.4197	11955208	0.5637
5621528	0.7991	8075991	1.2932	10027247	0.5887	12022407	0.7976
5685704	0.5129	8098178	0.9874	10324374	1.7311	12058533	0.3442
5771150	0.5049	8098228	0.5472	10384891	0.4079	12060710	0.3788
5937264	0.6037	8107903	1.5406	10403228	0.2369	12105694	1.9567
5938531	0.8800	8150479	0.3805	10412044	1.4002	12105867	1.1736
5951140	1.0551	8183594	0.2980	10462462	0.8696	12203082	0.5263
5952378	0.4528	8248415	0.9892	10469305	0.8971	12207432	1.6982
5962956	1.3998	8257134	0.2995	10515986	0.7472	12258225	0.9423
6102091	0.5162	8325962	0.5721	10518758	1.3394	12304013	0.3498
6117832	0.6047	8414250	0.7446	10536761	1.0255	12356535	0.8096
6122790	1.1193	8415004	1.2297	10552016	1.5089	12365719	0.8521
6183736	1.1819	8416220	0.5660	10553513	0.2547	12505054	0.4397
6370174	0.8606	8417053	1.4751	10584063	1.4280	12784183	0.2087
6425928	0.3255	8447096	1.2361	10587237	0.9603	12835232	1.8951
6469920	0.9717	8454353	1.4905	10677397	0.3115		
6529445	0.2231	8474897	0.9954	10710753	0.6493		

NOTE. — 178 *Kepler* targets exhibiting at least one starspot rotation period shorter than 2 days. If more than one period is present, only the shortest period is listed here. Periods are in days. For systems with more than one short rotation period see Table 2

TABLE 2
Kepler M STARS EXHIBITING TWO OR MORE SHORT ROTATION PERIODS

Object (1)	α_{J2000} (2)	δ_{J2000} (3)	K_p (4)	T_{eff} (5)	P_A (6)	P_B (7)	P_C (8)	P_D (9)	Imaging (10)
3454793	19h 36m 49.43s	38d 31m 47.50s	15.5	3431	0.6681	0.9673	UKIRT: elongated (?)
3757251	19h 36m 14.20s	38d 50m 19.25s	15.8	3623	0.2158	0.4485	15.40	...	UKIRT: 2.6'' & 4.2''
3831911	19h 00m 13.23s	38d 59m 06.04s	15.0	3953	0.5670	1.8343	30.484 [†]	...	UKIRT: 4.0''
3962433	19h 34m 28.26s	39d 01m 38.78s	15.8	3741	0.4024	0.6378	UKIRT: single
4077867	19h 45m 41.35s	39d 06m 34.56s	15.8	3490	0.4776	0.9798	19.35	...	UKIRT: 4.0''
4175707	19h 42m 47.72s	39d 16m 00.66s	15.0	3825	0.3406	0.4163	Keck AO: single
4264634	19h 28m 34.15s	39d 18m 00.76s	14.8	3939	0.7536	0.8865	12.38	...	UKIRT: single
4545041	19h 04m 19.82s	39d 37m 18.16s	15.9	3329	0.3321	0.4045	UKIRT: single
4660255	19h 33m 17.12s	39d 42m 32.62s	15.4	3917	0.4108	0.5251	0.7859	1.1958	UKIRT: elongated & 4.2''
5182822	19h 22m 00.25s	40d 22m 13.08s	15.7	3900	0.3390	1.1660	15.51	...	UKIRT: single
6425928	19h 01m 05.40s	41d 51m 29.38s	14.5	3862	0.3254	0.3942	2.4018	2.9842	UKIRT: single
6529445	19h 36m 05.46s	41d 56m 23.42s	15.7	3746	0.2231	0.2362	UKIRT: elongated & 4.7''
6936046	19h 10m 16.10s	42d 26m 36.49s	15.0	3772	0.5273	1.2327	13.21	...	UKIRT: 6.6'' [‡]
7110077	19h 17m 35.66s	42d 41m 37.28s	15.6	3598	0.9716	1.0390	22.08	...	UKIRT: 2 faint compan. at $\sim 1.3''$
7434110	19h 13m 24.06s	43d 02m 47.00s	16.0	3311	0.4014	1.8070	UKIRT: single
7448057	19h 31m 04.12s	43d 05m 54.96s	15.6	3500	0.3872*	1.9594	UKIRT: single
7449695	19h 32m 58.53s	43d 04m 42.92s	16.0	3787	0.5609	1.6635	UKIRT: single
7740983	19h 07m 57.37s	43d 29m 56.08s	14.7	3727	0.4036	0.5190	3.33	...	Keck AO: 0.32'' binary
7849619	19h 58m 02.71s	43d 34m 02.06s	15.5	3799	0.3092	0.3298	12.91	...	UKIRT: 2.6''
7973675	19h 45m 11.65s	43d 45m 26.50s	15.1	3506	0.4572	0.7764	17.40	...	UKIRT: single
8325962	19h 58m 46.21s	44d 15m 05.62s	15.0	3946	0.1690*	0.5719	7.721	12.34	UKIRT: 6.3''
8416220	19h 00m 57.66s	44d 28m 27.91s	15.1	3227	0.5659	0.7151	Keck AO: 0.27'' binary
8701179	19h 44m 31.15s	44d 53m 48.08s	15.9	3900	0.7046	0.7874	16.18	...	UKIRT: single
8873575	19h 07m 14.00s	45d 07m 40.12s	16.5	3906	0.6737	1.0226	11.88	...	UKIRT: single
8909833	19h 57m 23.98s	45d 09m 38.92s	15.6	3903	1.2802	7.385	11.80	...	UKIRT: 7'' & 11'' [‡]
9022001	19h 27m 18.51s	45d 22m 42.02s	16.0	3648	0.6989**	0.7055**	14.48	...	UKIRT: elongated & 4.0''
9268481	19h 02m 03.70s	45d 44m 06.76s	15.6	3198	0.5802*	1.5780	1.8638	...	UKIRT: single
9428095	19h 59m 37.83s	45d 56m 04.78s	15.9	3431	0.6289	0.6974	23.04	...	UKIRT: 3.0''
9519275	19h 14m 06.86s	46d 07m 18.77s	15.5	3578	0.5798	1.8706	17.71	...	UKIRT: 6''
9590249	19h 30m 58.54s	46d 13m 12.76s	15.8	3855	0.2640*	2.1665	12.0	...	UKIRT: single
10403228	19h 24m 54.41s	47d 32m 59.93s	16.1	3386	0.2367	0.2461	34.6	...	UKIRT: 2.8''
10584063	18h 57m 06.17s	47d 49m 28.67s	15.7	3316	1.397*	1.5988	18.72	...	UKIRT: single
10677397	19h 45m 09.30s	47d 54m 59.15s	15.3	3387	0.3115*	0.4743	7.803	...	UKIRT: double & 6'' & 7''
11955208	19h 06m 43.50s	50d 20m 08.77s	15.7	3604	0.5637	0.7028	1.1855	...	Keck AO: 0.1'' binary
12203082	19h 12m 51.12s	50d 48m 00.61s	15.3	3804	0.5263*	0.6592	11.75	...	UKIRT: single
12258225	19h 25m 41.94s	50d 56m 41.82s	14.7	3500	0.9416	1.0141	UKIRT: single
12304013	19h 17m 40.27s	51d 00m 16.92s	15.2	3465	0.3497	2.3491	19.12	...	UKIRT: single

NOTE. — * = inferred from only the base frequency and no higher harmonics; ** = sufficiently close that these may result from differential rotation of a single star; † - the period of an eccentric binary component of the system; (1) KIC ID, (2) Right Ascension, (3) Declination, (4) *Kepler* magnitude, K_p , (5) composite T_{eff} ; (6)–(9) rotation period in days, (10) Comments on the stellar neighbors inferred from the UKIRT J-band images, as well as the Keck AO images – where available; angular distances to some of the neighboring stars are noted. ‡ - the other stars are of a distinctly different, i.e., hotter, spectral type.